Journal of Materials Chemistry A

RSC Publishing

PAPER

Improvement of photovoltaic performance by ternary blending of amorphous and semi-crystalline polymer analogues with PCBM

Cite this: *J. Mater. Chem. A*, 2013, **1**, 3961

C. Kästner,*[a] S. Rathgeber,[b] D. A. M. Egbe[c] and H. Hoppe[a]

Received 12th November 2012
Accepted 18th January 2013

DOI: 10.1039/c3ta01070h

www.rsc.org/MaterialsA

Ternary blending of amorphous and semi-crystalline anthracene-containing poly(*p*-phenylene-ethynylene)-*alt*-poly(*p*-phenylene-vinylene) (PPE-PPV) copolymers (AnE-PVs) with PCBM was investigated in bulk heterojunction solar cells. In general, a strong impact on all photovoltaic parameters was observed by increasing the amount of amorphous AnE-PV*ba*-derivative in relation to its semi-crystalline counterpart AnE-PV*ab*. Interestingly, small additions of the amorphous copolymer were beneficial for overall solar cell performance. The observed performance increase of the ternary blend could be related to an improved open-circuit voltage, despite the fact that the binary blend of the amorphous copolymer and [6,6]-phenyl-C61-butyric acid methyl ester (PCBM) did not exhibit a larger photovoltage than the binary blend based on the semi-crystalline copolymer. These results indicate that a certain amorphous fraction of the donor polymer may be required for obtaining optimal bulk heterojunction morphologies, yielding maximum photovoltaic performance.

Introduction

Conjugated polymer based organic photovoltaics (P-OPV) has received increasing research[1–3] – and lately commercial[4] – interest, since it offers a flexible[5–7] and semitransparent[8–10] option for harvesting solar radiation at potentially low cost[11–13] and low-energy payback time.[14–16] The very successful development of OPV[17,18] over the last decade is based on the binary donor/acceptor bulk heterojunction concept,[19] where the electron donor (usually conjugated polymers) and electron acceptor (usually fullerene derivatives) are intimately blended on a nanometer scale. Furthermore, continued efforts in materials research, resulting in the development of improved donor polymers[20–22] as well as more suitable fullerene derivative acceptors,[23–25] resulted in a steady increase of device performance of binary donor/acceptor bulk heterojunction solar cells, approaching 10% power conversion efficiency (PCE) to date.[26]

The morphology of bulk heterojunctions based on polymer donor and fullerene derivative acceptor materials develops by self-organization and is influenced by many parameters that are not easily and only seldom separately controlled.[27,28] The impact of the bulk heterojunction nanomorphology on the device performance has already been reported by some early studies. In the case of amorphous PPV-derivatives the choice of solvent, from which the active layer was spin cast, determined largely the resulting PCE.[19,29–31] In the case of semi-crystalline poly(3-hexylthiophene) (P3HT), post-production treatments such as thermal annealing[32,33] or slow drying[34] improved the solar cell performance by enhanced structural ordering *i.e.* crystallization of P3HT.[35] Several approaches for controlling P3HT aggregation in solutions have already been pursued in order to yield an improved morphology control over the evolving bulk heterojunction.[36–40] For example, the formation of semi-crystalline P3HT fibers was achieved by addition of non-solvents into the P3HT-solution, resulting in a controlled aggregation of the polymer.[39,41] Interestingly, the best device performances have not been achieved with bulk heterojunctions containing solely semi-crystalline P3HT fibers as donor, but rather with a combination of fibers and some less ordered fraction of P3HT.[38,42]

This behaviour has recently been further investigated in ternary blends of regio-random and regio-regular P3HT in conjunction with [6,6]-phenyl-C61-butyric acid methyl ester (PCBM).[43] This ternary blend positively influenced the morphology as compared to devices based on binary blends. Due to the better miscibility of the amorphous regio-random P3HT with PCBM, long term morphological stability of the active layer was improved. However, no absolute improvement in the solar cell device performance was found.[43] On the other side, ternary blends of P3HT, PCBM and ICBA (indene-C60 bis-adduct) allowed the open-circuit voltage of the solar cells to be tuned linearly between the values obtained for the respective binary P3HT:PCBM and P3HT:ICBA blends.[44]

[a]*Institute of Physics, Ilmenau University of Technology, Langewiesener Str. 22, 98693 Ilmenau, Germany. E-mail: Christian.Kaestner@tu-ilmenau.de*

[b]*Institute for Natural Sciences, University Koblenz-Landau, Universitätsstr. 1, 56070 Koblenz, Germany*

[c]*Linz Institute for Organic Solar Cells, Johannes Kepler University Linz, Altenbergerstr. 69, 4040 Linz, Austria*

Hence ternary blending seems to be a promising approach for tuning certain properties of the bulk heterojunction that can otherwise not be obtained by using only two components. Further examples for the use of ternary blends were mostly motivated by a potential extension of the spectral sensitivity of polymer solar cells.[45–47] A rather large compatibility between all components of the ternary blends appears to be a prerequisite for the improvement of potential devices. A very systematic study on the miscibility of P3HT and PCPDTBT with PCBM and the corresponding solar cell device performances has been recently reported.[48] Again, no improvement over the binary bulk heterojunctions could be obtained, however, the evaluation of the ternary phase diagram provided information on the optimal blending ratio of all three components. Recently a performance improvement was obtained by ternary blending of $P3HT_{75}$-*co*-EHT_{25}, P3HTT-DPP-10% and PCBM as compared to the binary blends.[49] The ternary blend yielded a relative performance increase due to the complementary absorption of both polymers for small additions of $P3HT_{75}$-*co*-EHT_{25}.

Here we report about the use of two copolymers that are – due to an identical backbone – essentially the same polymer except for some modification on their side-chain substitution, leading to either semi-crystalline or amorphous properties. In contrast to P3HT an increase in structural order is found for the semi-crystalline version of the copolymer upon blending with the fullerene derivative acceptor PCBM.[40,50–52] Due to the similarity in the chemical structure, this system is particularly suited for investigating the effects concerned with controlling the order in ternary bulk heterojunctions.

It is generally proposed that pristine and rather well-ordered phases of donor polymers and acceptor fullerene derivatives yield superior charge transport properties in bulk heterojunctions at sufficient percolation and domain size.[53–55] Very recently it has been claimed that a disordered and amorphous donor–acceptor mixing phase may provide superior charge generation efficiencies due to a relative enhancement in the driving force for exciton dissociation.[56] If both, ordered charge transport "high-ways" and disordered exciton dissociation phases, can be combined, an additional benefit of the resulting bulk heterojunction morphology follows from an energetically hindered charge recombination.[57–60]

Experimental

Scheme 1 displays the chemical structure of the AnE-PV copolymers used in this study. AnE-PV*ab* and AnE-PV*ba* were synthesized as reported earlier[61] and used as electron donors within the bulk heterojunction. The electron acceptor PCBM was used as obtained from the supplier (Nano-C, USA). From wide-angle scattering experiments we know that AnE-PV*ab* is semi-crystalline whereas AnE-PV*ba* is amorphous.[62]

Thin films of pristine polymers and polymer:PCBM blends were spin cast under nitrogen atmosphere on glass substrates using 1 : 1 mixtures of chloroform–chlorobenzene solutions. Thin film absorption spectra were obtained with a Varian Cary 5000 UV/vis spectrophotometer using a 2-beam VW-setup for recording transmission and reflection. Thin film photoluminescence (PL) spectra were recorded with an Avantes avaspec 2048 fiber spectrometer over a wavelength range between 500 and 1100 nm, and normalized to the absorption value at the laser excitation wavelength of 405 nm.

Solar cell device preparation on glass involved etching part of the ITO-layer for selective contacting of the back electrode, followed by spin coating of PEDOT:PSS (Clevios PH, Heraeus). The PEDOT:PSS layers were annealed on a hot plate at 170 °C for 15 minutes in order to release water moieties. Thereafter the samples were transferred into a nitrogen (N_2) glovebox for further processing. Photoactive layers were spin cast from AnE-PV:PCBM solutions with a blend ratio of 2 : 3 by weight (polymer:PCBM) and a polymer concentration of 0.4 wt% under inert atmosphere. Spin frequencies were varied between 700 and 1300 rpm to obtain the optimum active layer thicknesses for each blend. The top aluminium electrode was deposited by physical vapor deposition in a vacuum chamber attached to the glovebox. Current–voltage (*I–V*) measurements of solar cell devices, exhibiting an active area of 0.5 cm^2, were recorded with a Keithley 2400 Source-Measure-Unit using a class A solar simulator (Solar Light, XPS 400). The external quantum efficiency (EQE) spectra were recorded using a bias illumination of an intensity equivalent to one sun. Neither solar cells nor thin films have been post-treated.

Film topography was characterized with a Veeco Dimension atomic force microscope (AFM) in tapping mode, using super sharp tips (TESP-SS).

Grazing incidence wide-angle X-ray scattering experiments were performed at the BW4 beam line, at HASYLAB at DESY in Hamburg, Germany. Experiments were carried out in a pseudo-grazing incidence configuration at a wavelength of $\lambda = 0.138$ nm, a band width of 10^{-4} and a spot size of 78 μm × 46 μm in the horizontal and vertical direction, respectively. The incident polar angle has been set to $\alpha_i = 0.20°$ for probing the full film cross-section. Surface sensitive measurements were taken at an incident angle of $\alpha_i = 0.10°$, which is below the critical angle of the active layer. Two-dimensional detector patterns were collected with an exposure time of 900 s on a CCD-detector (MAR165CCD, pixel size 79.1 μm). The detector to sample distance was determined by means of a silver behenate standard. Data were corrected for background scattering from the quartz glass substrate and were normalized to the incoming flux and film thicknesses ($\alpha_i = 0.20°$ only) in order to allow for a comparison of peak intensities between different samples. All GiWAXS plots are shown as one-dimensional detector cuts, intensity versus q, where $q = 2\pi/d$ is the overall momentum transfer which can be directly related to the distance d of the corresponding scattering planes. Detector cuts were taken through the interlayer peaks in q_z direction (momentum transfer perpendicular to the surface plane) and for the detection of the isotropic scattering contributions the two-dimensional data were averaged over all angles Φ between q_z and q_p (momentum transfer parallel to the surface plane). For more details on the experimental setup and data conversion see ref. 52.

Results and discussion

Fig. 1 displays the optical properties, absorption and photoluminescence spectra of the binary AnE-PV (a and b) and ternary

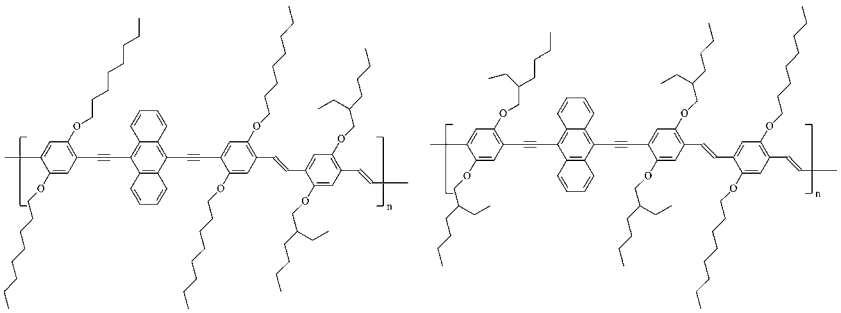

Scheme 1 The molecular structure of the AnE-PV copolymers: on the left, AnE-PV*ab*, the semi-crystalline version, and on the right, AnE-PV*ba*, the amorphous one.

AnE-PV:PCBM (c and d) films. Spectra were taken for different blend ratios of semi-crystalline AnE-PV*ab* and amorphous AnE-PV*ba*. The polymer ratio was varied in steps of 10 wt% between pristine AnE-PV*ab* (0% *ba*) and pristine AnE-PV*ba* (100% *ba*).

The absorption spectra of the polymer films appear to be almost additive according to the different composition ratios between semi-crystalline AnE-PV*ab* and amorphous AnE-PV*ba* in the binary polymer blends, thus indicating energetically undisturbed mixing and – if any – only weak intermolecular interactions. The higher order of the semi-crystalline version, AnE-PV*ab*, is reflected by the relative proportion of the two lowest absorption peaks located at 580 nm and 550 nm (ref. 63 and 64) whereas the disorder of amorphous AnE-PV*ba* is reflected by a single broad and blue-shifted absorption peak centered around 520 nm. In agreement with the absorption spectra, the photoluminescence of the pristine AnE-PV*ba* is blue-shifted relative to the one observed for the AnE-PV*ab* and binary blends of the two. In addition, the luminescent emission of the binary polymer blends is smoothly varying between the limiting values of pristine AnE-PV*ba* and -*ab*. Interestingly, the normalized PL intensity is larger for all binary polymer blends as compared to the pristine single-component polymer films.

Similarly, the absorption of the ternary AnE-PV:PCBM blends smoothly varied between the spectra of the binary AnE-PV:PCBM blends, indicating again undisturbed mixing. However, in contrast to the polymer films, the order – corresponding to the

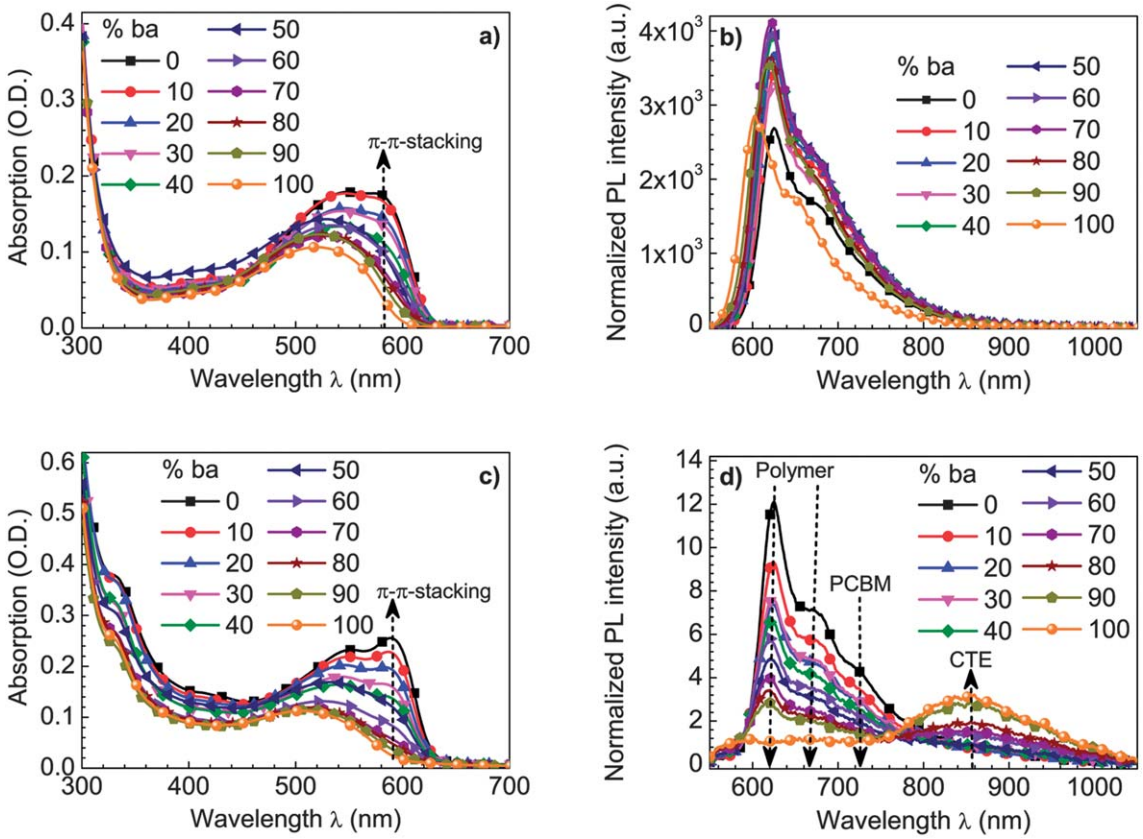

Fig. 1 Thin film absorption and normalized PL spectra of binary AnE-PV (a and b) and ternary AnE-PV:PCBM (2 : 3) (c and d) blends. Polymer compositions are indicated by the weight fraction of AnE-PV*ba* (% *ba*) within the binary polymer part of the ternary blend system.

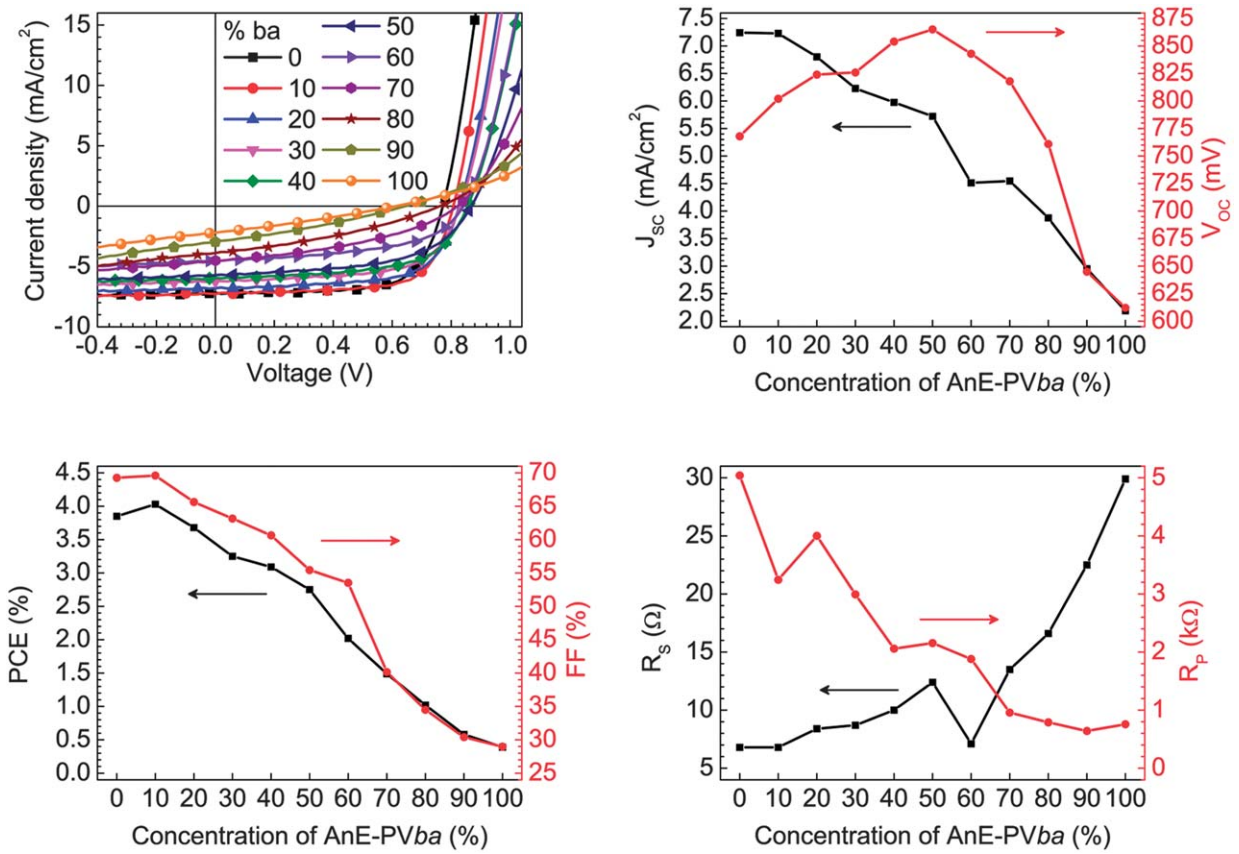

Fig. 2 *J–V* characteristics and compositional dependence of photovoltaic parameters (J_{SC}, V_{OC}, FF, PCE, R_S, R_P) of devices prepared from binary and ternary AnE-PV:PCBM blends. The parameters are plotted versus the concentration of the amorphous polymer within the donor-phase of the bulk heterojunction. The total AnE-PV:PCBM blend ratio was 2 : 3 by weight.

two low-energy absorption peaks of AnE-PV*ab* – is increased within the blends with PCBM. This observation implies that the addition of the fullerene derivative did not disturb the order – as in the case of regio-regular P3HT[40,50,51] – but rather promotes aggregation and crystallization of the semi-crystalline AnE-PV*ab*. The exact reason for the enhanced crystallization is currently unresolved, however, it can be hypothesized that the relative or partial solution concentration of the copolymer is increased upon addition of PCBM within the common solvent. Indeed, for higher concentrated solutions the free energy can be better minimized under formation of aggregates – or in other words, semi-crystalline polymers are more prone to aggregation in more concentrated solutions.[37,65]

Also the photoluminescence spectra of the ternary AnE-PV:PCBM bulk heterojunctions seem to be, by large extent, almost a linear superposition of the corresponding binary AnE-PV:PCBM blends. Deviations from that linearity are found for very small or large AnE-PV*ba* concentrations. The bulk heterojunction based on semi-crystalline AnE-PV*ab* exhibits a reduced PL-spectrum by about 3 orders of magnitude, closely corresponding to the one obtained for the pristine polymer film. However, the amorphous AnE-PV*ba*:PCBM PL-spectrum exhibits new features at considerably longer wavelengths, but no photoluminescence originating from the pristine polymer. These red-shifted emissions can be attributed to a charge transfer (CT) recombination between electrons located at a PCBM molecule and holes located on the polymer.[66–68] The occurrence of this CT-state photoluminescence has already been attributed to constitute a loss-channel for otherwise potentially current contributing charge carriers in P3HT-based bulk heterojunctions.[68] It should be noted that this CT-peak starts to become noticeable for AnE-PV*ba* concentrations

Table 1 Compositional dependence of photovoltaic parameters for binary and ternary AnE-PV:PCBM blends. The AnE-PV:PCBM blend ratio was 2 : 3 by weight, independent of the polymer composition. The fraction of amorphous AnE-PV*ba* (wt%) within the polymer donor-phase is listed in the left column

ba (%)	J_{SC} (mA cm^{-2})	V_{OC} (mV)	FF (%)	PCE (%)	R_S (Ω)	R_P (kΩ)
0	7.24	768	69.26	3.85	6.8	5.04
10	7.23	802	69.60	4.03	6.8	3.24
20	6.80	824	65.63	3.68	8.4	4.00
30	6.23	826	63.16	3.25	8.7	2.99
40	5.98	854	60.64	3.09	10.0	2.06
50	5.72	865	55.44	2.75	12.4	2.16
60	4.51	843	53.52	2.02	7.1	1.88
70	4.55	818	40.16	1.49	13.5	0.96
80	3.88	761	34.50	1.02	16.6	0.79
90	2.95	645	30.41	0.58	22.5	0.64
100	2.19	612	28.97	0.39	29.9	0.76

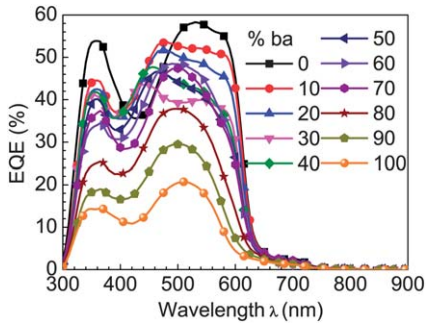

Fig. 3 EQE spectra of solar cell devices prepared from binary and ternary AnE-PV:PCBM (2 : 3) blends with various compositions of the polymer donor-phase, recorded under bias illumination with an intensity corresponding to one sun.

between 30–40%. Since a non-negligible photoluminescence contribution of AnE-PV*ab* is observed for all blends containing the semi-crystalline polymer, the semi-crystalline phase appears to develop nearly undisturbed by the presence of the amorphous polymer, always resulting in a certain domain size in which not all excitons can reach the heterojunction and get dissociated. The photoluminescence spectra of the donor–acceptor bulk heterojunctions thus indicate clearly that semi-crystalline AnE-PV*ab* is significantly phase-separating from PCBM, whereas amorphous AnE-PV*ba* shows a comparably larger tendency of intimately mixing with PCBM. For the binary or ternary bulk heterojunctions containing no or little AnE-PV*ba*, another PL-peak above 700 nm was detected. This PL-feature has to be attributed to radiative recombination of excitons within a pristine PCBM phase that were not able to reach the heterojunction interface. In summary, the presence of photoluminescence signals from pristine AnE-PV*ab* and PCBM phases provides a clear indication for significant phase separation between AnE-PV*ab* and PCBM.[30,69] Increasing amounts of amorphous AnE-PV*ba* result in an intimate mixture with the PCBM, thus eliminating pristine PCBM phases by improved miscibility and provoking massive CT-recombination across the heterojunction.

Complementary, combined electro-optical investigations were performed by fabrication and characterization of solar cell devices based on bulk heterojunctions prepared from the same blends.

Table 1 depicts the photovoltaic parameters of thickness optimized devices obtained from binary and ternary AnE-PV:PCBM blends. Fig. 2 visualizes these photovoltaic parameters as a function of the relative AnE-PV*ba* concentration with respect to AnE-PV*ab*. Indeed, changing the blend ratio between the semi-crystalline and the amorphous polymer in the ternary bulk heterojunctions resulted in a steady and systematic variation of all photovoltaic parameters. A relatively large power conversion efficiency was found for the active layer containing no amorphous polymer, whereas the smallest was obtained, if solely amorphous polymer was used. This is in good agreement with earlier studies conducted on regio-regular and regio-random P3HT, accordingly.[61,70] Both polymers exhibit comparably low open-circuit voltages (V_{OC}) in the binary blends. The open-circuit voltage of the ternary blends increased progressively with the concentration of amorphous AnE-PV*ba* up to 50 wt% and decreased thereafter again for higher concentrations, indicating losses due to increased charge recombination.[71]

Intriguingly, the largest fill factor (FF) and overall device efficiency were obtained for blending AnE-PV*ab* with 10 wt% of amorphous AnE-PV*ba*. This performance increase for the ternary blend was due to a similar photocurrent, but slightly increased the open-circuit voltage and fill factor as compared to the binary bulk heterojunction based solely on semi-crystalline AnE-PV*ab* and PCBM. At larger concentrations of AnE-PV*ba*, both, fill factor and photocurrent, decreased steadily. The

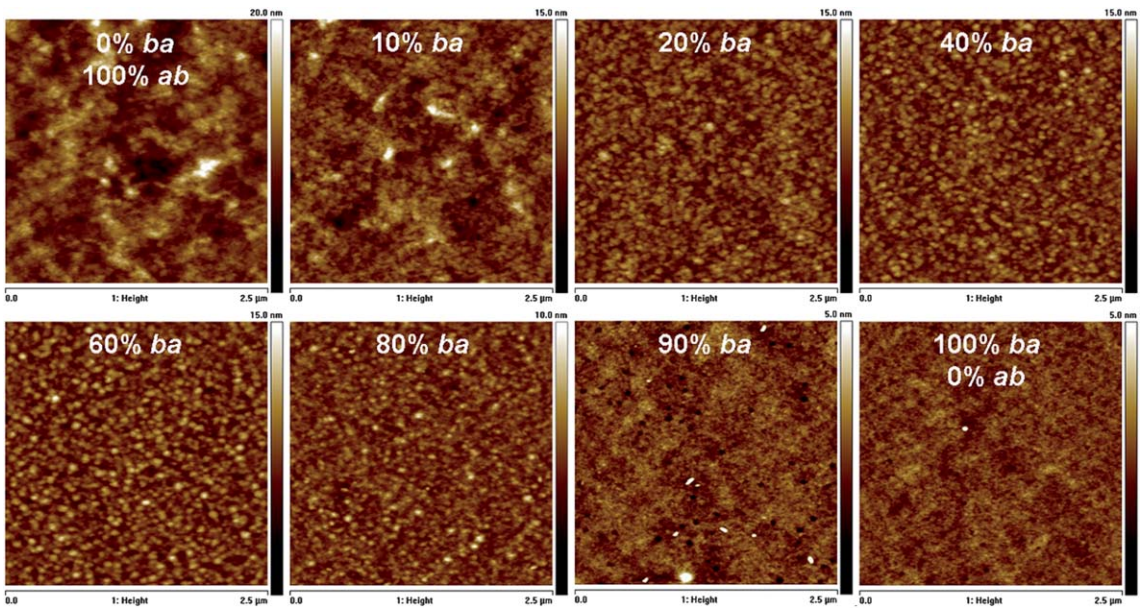

Fig. 4 AFM tapping mode topography images of thin films spin cast from binary and ternary AnE-PV:PCBM blend solutions with varying composition of the polymer donor-fraction.

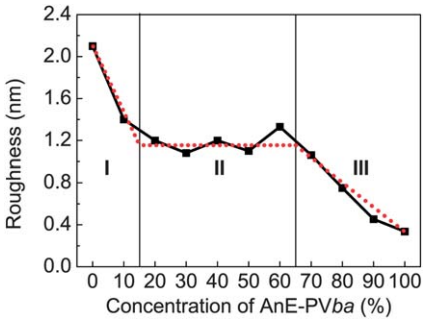

Fig. 5 RMS surface roughness determined by AFM on thin binary and ternary AnE-PV:PCBM blend films. Three regimes of phase separation can be identified: (I) large scale, (II) constant and (III) diminishing roughness.

reduced fill factor, efficiency and short-circuit current density (J_{SC}) at AnE-PV*ba* concentrations above 10 wt% are in accordance with increasing recombination losses as detected *via* the pronounced CT loss signal (750 nm to 1050 nm) of the AnE-PV:PCBM blend PL spectra.[68] Furthermore, the decreasing volume fraction of the coarse-grained (well phase-separated) semi-crystalline polymer as deduced from the PL spectra implies reduced hole percolation and consequently larger recombination rates.[69] The reduction in charge conductivity with increasing fraction of amorphous AnE-PV*ba* is also strongly reflected by the steady increase of the series resistance (R_S) over the whole concentration range. On the other hand, the parallel resistance (R_P) decreased severely with increasing AnE-PV*ba* concentration. For very high AnE-PV*ba* concentrations, the optimization yielded relatively thin active layers due to the large series resistance, and therefore the parallel resistance was so low that partial shunting of the devices could not fully be excluded.

All EQE spectra of the investigated binary and ternary AnE-PV:PCBM blend systems were recorded under bias illumination with an intensity corresponding to one sun and are presented in Fig. 3. The EQE spectra are in good quantitative agreement with the observed short-circuit current densities.

The pristine AnE-PV*ab* blended with PCBM exhibited the largest EQE for both, the polymer and the PCBM fraction. Admixture of amorphous AnE-PV*ba* decreased the EQE, but an additional contribution between 420 nm and 480 nm is observed. This could at least in part be attributed to the blue-

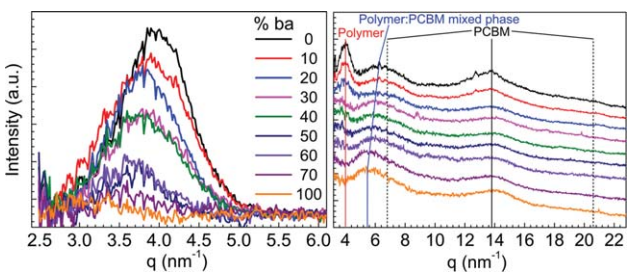

Fig. 6 Surface sensitive GiWAXS results ($\alpha_i = 0.10°$) for various concentrations of AnE-PV*ba* in the binary and ternary AnE-PV:PCBM blend films: detector cuts taken through the interlayer peak (left) and averaged over the full Φ-range (right).

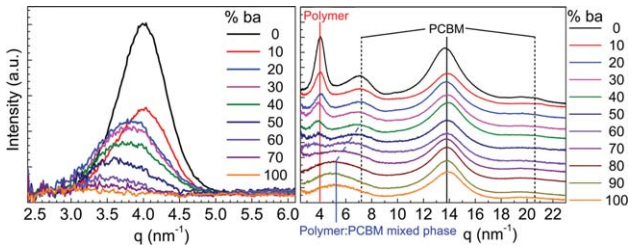

Fig. 7 GiWAXS results probing the full film cross-sections ($\alpha_i = 0.20°$) for various concentrations of AnE-PV*ba* in the binary and ternary AnE-PV:PCBM blend films: detector cuts taken through the interlayer peak (left) and averaged over the full Φ-range (right).

shifted absorption of the amorphous polymer fraction. For an AnE-PV*ba* fraction of only 10 wt% this additional contribution balances almost quantitatively the relative 10% loss at the corresponding maxima of the polymer and PCBM contribution to the EQE. Further increase of AnE-PV*ba* concentration lead to steady decrease in the overall EQE in accordance with the short-circuit photocurrent obtained from the *J–V* characteristics.

Interestingly, an addition of only 10% of the amorphous and disordered AnE-PV*ba* resulted in an overall power conversion efficiency increase. The thereby increased volume fraction of the amorphous and intimately mixed AnE-PV:PCBM phase is most likely located between the pristine semi-crystalline phases of the ordered AnE-PV*ab* and PCBM. Thus the separation between the molecular energy levels within the amorphous phase increases due to disorder,[60] which potentially yields an improvement in the open-circuit voltage and also in the fill factor, as it may act as a barrier for charge recombination.[57]

To gain deeper insight into the nanomorphology of AnE-PV*ab*:AnE-PV*ba*:PCBM blend films, structural information was obtained by AFM topography and GiWAXS measurements. Fig. 4 depicts the AFM tapping mode images of thin films spin cast from binary and ternary AnE-PV:PCBM blend solutions with varying donor composition.

The composition of the ternary AnE-PV*ab*:AnE-PV*ba*:PCBM blends had a strong impact on the evolution of the topography. The roughest topography, indicating pronounced self-organization of the polymer as well as the formation of larger PCBM

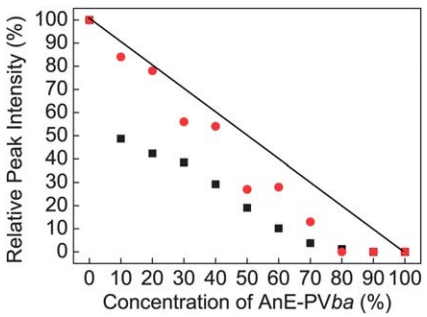

Fig. 8 Relative peak intensities of the AnE-PV*ab* interlayer peaks as a function of the AnE-PV*ba* concentration: surface sensitive measurements ($\alpha_i = 0.10°$, Fig. 6 left) (red circles) and those obtained from the full film cross-section ($\alpha_i = 0.20°$, Fig. 7 left) (black squares). Peak intensities are normalized to those obtained for the binary AnE-PV*ab*:PCBM film.

aggregates, was found for the binary blend based on the pristine AnE-PV*ab*. By addition of amorphous AnE-PV*ba* the surface roughness decreased considerably. Further increase of the AnE-PV*ba* concentration resulted in a coarse-grained structure, which indicates certain domain size of a single phase. Interestingly, this topography appears to be widely independent of the composition of semi-crystalline and amorphous AnE-PV up to about 70% of AnE-PV*ba*. For higher concentrations of amorphous AnE-PV*ba* the surface morphology became smoother and the grainy structures disappeared. The featureless surface morphology of AnE-PV*ba* reflects strong intermixing of AnE-PV*ba* and PCBM. The root mean square (RMS) surface roughness of all characterized films is plotted in Fig. 5 and provides a rough measure of the phase separation between both AnE-PVs and PCBM.

The graph illustrates the three regimes of phase separation discussed above: (I) strong phase separation between AnE-PV*ab* and PCBM controlled by self-aggregation of the nearly pristine semi-crystalline AnE-PV*ab* and large PCBM aggregates, (II) intermediate phase separation widely independent of the AnE-PV*ba* concentration, and (III) smooth blending controlled by intimate mixing of AnE-PV*ba* and PCBM. These findings are in good agreement with the absorption and luminescence spectroscopy results: semi-crystalline AnE-PV*ab* promotes phase separation, whilst amorphous AnE-PV*ba* tends to intimately mix with PCBM. The three regimes deduced from the topography measurements can be roughly correlated with the results obtained from optical spectroscopy: The first regime of strong phase separation is in accordance with the observation of the two photoluminescence signals of pristine AnE-PV*ab* and PCBM. The principal agreement for the second regime is less obvious, as in the optical properties a smooth variation in the order (absorption) and volume fraction of larger domains (photoluminescence) is detected, whereas the topography shows little or no variations. The last regime, corresponding to intimate mixing of AnE-PV*ba* and PCBM, is well reflected by the loss of any detectable order in the absorption and by the strong appearance of CT-photoluminescence. The differences between topography and optical spectroscopy for the intermediate regime (II) are to be related to differences in the bulk (spectroscopy) and surface (topography) properties of the blend films.

In order to analyze whether there is a difference in morphology evolution at the surface and in the bulk of the blend films, we further studied the structure of binary and ternary AnE-PV:PCBM based bulk heterojunctions by GiWAXS close to the free surface ($\alpha_i = 0.10°$, Fig. 6) as well as averaged over the full film cross-section ($\alpha_i = 0.20°$, Fig. 7). Fig. 8 compares the intensities of the interlayer peaks originating from the semi-crystalline AnE-PV*ab* obtained for the free surface to those obtained for the film "bulk" as a function of the AnE-PV*ba* concentration. Indeed, the scattering results depict that the addition of a small amount of amorphous polymer AnE-PV*ba* affects the order of the polymer -*ab* much stronger in the "bulk" of the bulk heterojunction than on its free surface.

At the free surface the peak intensities of the interlayer peaks decreased up to an AnE-PV*ba* concentration of 40% almost according to the dependence expected for a decreasing AnE-PV*ab* fraction (see solid black line in Fig. 8). Above this concentration there is a significant drop in the peak intensities and from an AnE-PV*ba* fraction of about 80% no residual scattering from the AnE-PV*ab* interlayer ordering is detectable. The intensity of the main PCBM peak at $q = 14\ nm^{-1}$, detecting nearest neighbour correlations (solid black line in Fig. 7), is taken as a measure for the degree of phase separation. The degree of phase separation is generally low. The dashed solid lines mark the location where typically higher order scattering contributions from PCBM show up. Those were not detectable. The signal intensity of the main PCBM peak decreased from an AnE-PV*ba* concentration of 0% to 20% and then remained constant, which is in accordance with the general development of the film roughness (AFM) and the trend of the PCBM PL-signal. The additional scattering feature at around 6 nm^{-1} (0% AnE-PV*ba*) and 5 nm^{-1} (100% AnE-PV*ba*) cannot be assigned to a known PCBM peak. Its intensity is indeed comparable to that of the main PCBM peak at $q = 14\ nm^{-1}$, which should be the most prominent scattering feature of PCBM. Since the corresponding dimensions in real space are smaller than the polymer interlayer stacking distance but larger than the inter-PCBM-distances, we suggest that this peak originates from an AnE-PV:PCBM mixed phase with short-range order only, where the PCBM is preferably intercalated between virtual π-π-stacks.

For the film "bulk" spectra we observed a significant drop in the interlayer peak intensities upon addition of a small amount of only 10% AnE-PV*ba*. Further increase of the AnE-PV*ba* concentration lead to an almost linear dependence of the peak intensities as expected for a decreasing AnE-PV*ab* fraction. As for the surface sensitive measurements at AnE-PV*ba* concentrations above 80% no interlayer stacking order from the AnE-PV*ab* polymer was detected anymore.

The degree of phase separation and order are high in the binary mixture of AnE-PV*ab*:PCBM. The intensity of the main PCBM peak drops significantly upon addition of a small amount (10%) of amorphous AnE-PV*ba*. This is in accordance with the significant drop in the interlayer peak intensity which is most likely due to the formation of an intercalated, amorphous AnE-PV:PCBM phase. Typical higher order PCBM scattering features are detectable up to about 40% concentration of AnE-PV*ba*. At higher AnE-PV*ab* concentrations the main PCBM peak does not further decrease, indicating a certain remaining fraction of pristine PCBM phase at all AnE-PV compositions. Similar to the results obtained from the surface sensitive measurements at higher AnE-PV*ba* concentrations a peak at about 5 nm^{-1} appears which can be most likely attributed to a new intercalated phase with short-range order only, where the PCBM is preferably intercalated between virtual π-π-stacks. Thus, in sum the intercalated phase becomes more pronounced with increasing amorphous polymer fraction. The development of the new intercalated phase might be responsible for the massive CT-recombination losses at high AnE-PV*ba* concentrations as deduced from the PL spectra.

In summary, the presence of neat crystalline polymer and PCBM phases in combination with a small amount of the intimately intermixed, amorphous polymer:PCBM phase seem to

be a requirement in the design of active layer nanomorphologies providing highly efficient charge generation and extraction.[57]

Conclusion

We demonstrate an absolute improvement in photovoltaic performance of bulk heterojunction solar cells based on ternary blending of semi-crystalline and amorphous PPE-PPV copolymers, which are just bearing different side-chains, with PCBM. Blends of highly ordered AnE-PV*ab* and small amounts of amorphous AnE-PV*ba* lead to a beneficial bulk heterojunction morphology containing an ordered hole and electron conducting phase as well as an intimately mixed, amorphous AnE-PV:PCBM phase. In general a strong dependence of photovoltaic parameters on the ratio of ordered and amorphous polymers was found. We assign the local maximum at small amorphous polymer fraction to modifications of the AnE-PV:PCBM interface, in which the mixed amorphous blend most likely is located in between pristine ordered AnE-PV and PCBM phases. Further structural, electrical and optical investigations are required for a deeper understanding of the impact of nanomorphology onto charge carrier generation, recombination and transport in such ternary polymer:polymer:fullerene systems and will be addressed in the near future.

Acknowledgements

The authors are grateful to the Deutsche Forschungsgemeinschaft (DFG) for financial support in the framework of the priority program SPP1355.

References

1 P. Kumar and S. Chand, *Prog. Photovoltaics*, 2012, **20**, 377–415.
2 G. Li, R. Zhu and Y. Yang, *Nat. Photonics*, 2012, **6**, 153–161.
3 W. Yanmin, *J. Sol. Energy Eng.*, 2012, **134**, 011017.
4 http://www.neubers.de.
5 T. T. Larsen-Olsen, F. Machui, B. Lechene, S. Berny, D. Angmo, R. Soslashndergaard, N. Blouin, W. Mitchell, S. Tierney, T. Cull, P. Tiwana, F. Meyer, M. Carrasco-Orozco, A. Scheel, W. Loumlvenich, R. de Bettignies, C. J. Brabec and F. C. Krebs, *Adv. Energy Mater.*, 2012, **2**, 1091–1094.
6 F. C. Krebs, S. A. Gevorgyan and J. Alstrup, *J. Mater. Chem.*, 2009, **19**, 5442–5451.
7 F. C. Krebs, M. Jorgensen, K. Norrman, O. Hagemann, J. Alstrup, T. D. Nielsen, J. Fyenbo, K. Larsen and J. Kristensen, *Sol. Energy Mater. Sol. Cells*, 2009, **93**, 422–441.
8 G.-M. Ng, E. L. Kietzke, T. Kietzke, L.-W. Tan, P.-K. Liew and F. Zhu, *Appl. Phys. Lett.*, 2007, **90**, 103505-1–103505-3.
9 T. Ameri, G. Dennler, C. Waldauf, H. Azimi, A. Seemann, K. Forberich, J. Hauch, M. Scharber, K. Hingerl and C. J. Brabec, *Adv. Funct. Mater.*, 2010, **20**, 1592–1598.
10 D. Han, H. Kim, S. Lee, M. Seo and S. Yoo, *Opt. Express*, 2010, **18**, A513–A521.
11 S. E. Shaheen, D. S. Ginley and G. E. Jabbour, *MRS Bull.*, 2005, **30**, 10–19.
12 E. Ahlswede, W. Muehleisen, M. W. b. M. Wahi, J. Hanisch and M. Powalla, *Appl. Phys. Lett.*, 2008, **92**, 143307-1–143307-3.
13 S.-I. Na, B.-K. Yu, S.-S. Kim, D. Vak, T.-S. Kim, J.-S. Yeo and D.-Y. Kim, *Sol. Energy Mater. Sol. Cells*, 2010, **94**, 1333–1337.
14 T. D. Nielsen, C. Cruickshank, S. Foged, J. Thorsen and F. C. Krebs, *Sol. Energy Mater. Sol. Cells*, 2010, **94**, 1553–1571.
15 N. Espinosa, M. Hosel, D. Angmo and F. C. Krebs, *Energy Environ. Sci.*, 2012, **5**, 5117–5132.
16 N. Espinosa, R. Garcia-Valverde and F. C. Krebs, *Energy Environ. Sci.*, 2011, **4**, 1547–1557.
17 M. A. Green, K. Emery, Y. Hishikawa, W. Warta and E. D. Dunlop, *Prog. Photovoltaics*, 2012, **20**, 606–614.
18 Y. Y. Liang, Z. Xu, J. B. Xia, S. T. Tsai, Y. Wu, G. Li, C. Ray and L. P. Yu, *Adv. Mater.*, 2011, **22**, 135–138.
19 G. Yu, J. Gao, J. C. Hummelen, F. Wudl and A. J. Heeger, *Science*, 1995, **270**, 1789–1791.
20 D. Gendron and M. Leclerc, *Energy Environ. Sci.*, 2011, **4**, 1225–1237.
21 P. M. Beaujuge and J. M. J. Frechet, *J. Am. Chem. Soc.*, 2011, **133**, 20009–20029.
22 H. X. Zhou, L. Q. Yang and W. You, *Macromolecules*, 2012, **45**, 607–632.
23 F. B. Kooistra, J. Knol, F. Kastenberg, L. M. Popescu, W. J. H. Verhees, J. M. Kroon and J. C. Hummelen, *Org. Lett.*, 2007, **9**, 551–554.
24 P. A. Troshin, H. Hoppe, J. Renz, M. Egginger, J. Y. Mayorova, A. E. Goryochev, A. S. Peregudov, R. N. Lyubovskaya, G. Gobsch, N. S. Sariciftci and V. F. Razumov, *Adv. Funct. Mater.*, 2009, **19**, 779–788.
25 Y. J. He and Y. F. Li, *Phys. Chem. Chem. Phys.*, 2011, **13**, 1970–1983.
26 M. A. Green, *Prog. Photovoltaics*, 2012, **20**, 472–476.
27 E. Moons, *J. Phys.: Condens. Matter*, 2002, **14**, 12235–12260.
28 H. Hoppe and N. S. Sariciftci, *J. Mater. Chem.*, 2006, **16**, 45–61.
29 S. E. Shaheen, R. Radspinner, N. Peyghambarian and G. E. Jabbour, *Appl. Phys. Lett.*, 2001, **79**, 2996–2998.
30 H. Hoppe, M. Niggemann, C. Winder, J. Kraut, R. Hiesgen, A. Hinsch, D. Meissner and N. S. Sariciftci, *Adv. Funct. Mater.*, 2004, **14**, 1005–1011.
31 H. Hoppe, D. A. M. Egbe, D. Muhlbacher and N. S. Sariciftci, *J. Mater. Chem.*, 2004, **14**, 3462–3467.
32 F. Padinger, R. S. Rittberger and N. S. Sariciftci, *Adv. Funct. Mater.*, 2003, **13**, 85–88.
33 W. L. Ma, C. Y. Yang, X. Gong, K. Lee and A. J. Heeger, *Adv. Funct. Mater.*, 2005, **15**, 1617–1622.
34 G. Li, V. Shrotriya, J. S. Huang, Y. Yao, T. Moriarty, K. Emery and Y. Yang, *Nat. Mater.*, 2005, **4**, 864–868.
35 X. N. Yang, J. Loos, S. C. Veenstra, W. J. H. Verhees, M. M. Wienk, J. M. Kroon, M. A. J. Michels and R. A. J. Janssen, *Nano Lett.*, 2005, **5**, 579–583.
36 N. Kiriy, E. Jahne, H. J. Adler, M. Schneider, A. Kiriy, G. Gorodyska, S. Minko, D. Jehnichen, P. Simon, A. A. Fokin and M. Stamm, *Nano Lett.*, 2003, **3**, 707–712.

37 W. Y. Huang, P. T. Huang, Y. K. Han, C. C. Lee, T. L. Hsieh and M. Y. Chang, *Macromolecules*, 2008, **41**, 7485–7489.
38 A. J. Moule and K. Meerholz, *Adv. Mater.*, 2008, **20**, 240–245.
39 S. Y. Sun, T. Salim, L. H. Wong, Y. L. Foo, F. Boey and Y. M. Lam, *J. Mater. Chem.*, 2011, **21**, 377–386.
40 M. J. Sobkowicz, R. L. Jones, R. J. Kline and D. M. DeLongchamp, *Macromolecules*, 2012, **45**, 1046–1055.
41 H. Yan, Y. Yan, Z. Yu and Z. Wei, *J. Phys. Chem. C*, 2011, **115**, 3257–3262.
42 S. Berson, R. De Bettignies, S. Bailly and S. Guillerez, *Adv. Funct. Mater.*, 2007, **17**, 1377–1384.
43 M. Campoy-Quiles, Y. Kanai, A. El-Basaty, H. Sakai and H. Murata, *Org. Electron.*, 2009, **10**, 1120–1132.
44 P. P. Khlyabich, B. Burkhart and B. C. Thompson, *J. Am. Chem. Soc.*, 2011, **133**, 14534–14537.
45 N. A. Cooling, X. Zhou, T. A. Sales, S. E. Sauer, S. J. Lind, K. C. Gordon, T. W. Jones, K. B. Burke, P. C. Dastoor and W. J. Belcher, *Sol. Energy Mater. Sol. Cells*, 2012, **98**, 308–316.
46 S. Honda, H. Ohkita, H. Benten and S. Ito, *Adv. Energy Mater.*, 2011, **1**, 588–598.
47 M. Stavytska-Barba, M. Salvador, A. Kulkarni, D. S. Ginger and A. M. Kelley, *J. Phys. Chem. C*, 2011, **115**, 20788–20794.
48 F. Machui, S. Rathgeber, N. Li, T. Ameri and C. J. Brabec, *J. Mater. Chem.*, 2012, **22**, 15570–15577.
49 P. P. Khlyabich, B. Burkhart and B. C. Thompson, *J. Am. Chem. Soc.*, 2012, **134**, 9074–9077.
50 S. Engmann, V. Turkovic, G. Gobsch and H. Hoppe, *Adv. Energy Mater.*, 2011, **1**, 684–689.
51 S. Engmann, V. Turkovic, P. Denner, H. Hoppe and G. Gobsch, *J. Polym. Sci., Part B: Polym. Phys.*, 2012, **50**, 1363–1373.
52 S. Rathgeber, J. Perlich, F. Kuhnlenz, S. Turk, D. A. M. Egbe, H. Hoppe and R. Gehrke, *Polymer*, 2011, **52**, 3819–3826.
53 H. Sirringhaus, P. J. Brown, R. H. Friend, M. M. Nielsen, K. Bechgaard, B. M. W. Langeveld-Voss, A. J. H. Spiering, R. A. J. Janssen, E. W. Meijer, P. Herwig and D. M. de Leeuw, *Nature*, 1999, **401**, 685–688.
54 I. McCulloch, M. Heeney, C. Bailey, K. Genevicius, I. Macdonald, M. Shkunov, D. Sparrowe, S. Tierney, R. Wagner, W. M. Zhang, M. L. Chabinyc, R. J. Kline, M. D. McGehee and M. F. Toney, *Nat. Mater.*, 2006, **5**, 328–333.
55 A. R. Aiyar, J. I. Hong and E. Reichmanis, *Chem. Mater.*, 2012, **24**, 2845–2853.
56 H. Ohkita, S. Cook, Y. Astuti, W. Duffy, S. Tierney, W. Zhang, M. Heeney, I. McCulloch, J. Nelson, D. D. C. Bradley and J. R. Durrant, *J. Am. Chem. Soc.*, 2008, **130**, 3030–3042.
57 F. C. Jamieson, E. B. Domingo, T. McCarthy-Ward, M. Heeney, N. Stingelin and J. R. Durrant, *Chem. Sci.*, 2012, **3**, 485–492.
58 R. Osterbacka, C. P. An, X. M. Jiang and Z. V. Vardeny, *Science*, 2000, **287**, 839–842.
59 X. M. Jiang, R. Osterbacka, O. Korovyanko, C. P. An, B. Horovitz, R. A. J. Janssen and Z. V. Vardeny, *Adv. Funct. Mater.*, 2002, **12**, 587–597.
60 I. W. Hwang, D. Moses and A. J. Heeger, *J. Phys. Chem. C*, 2008, **112**, 4350–4354.
61 D. A. M. Egbe, S. Turk, S. Rathgeber, F. Kuhnlenz, R. Jadhav, A. Wild, E. Birckner, G. Adam, A. Pivrikas, V. Cimrova, G. Knor, N. S. Sariciftci and H. Hoppe, *Macromolecules*, 2010, **43**, 1261–1269.
62 S. Rathgeber, D. B. de Toledo, E. Birckner, H. Hoppe and D. A. M. Egbe, *Macromolecules*, 2010, **43**, 306–315.
63 F. C. Spano, *J. Chem. Phys.*, 2005, **122**, 234701-1–234701-15.
64 J. Clark, C. Silva, R. H. Friend and F. C. Spano, *Phys. Rev. Lett.*, 2007, **98**, 206406-1–206406-4.
65 T. Q. Nguyen, V. Doan and B. J. Schwartz, *J. Chem. Phys.*, 1999, **110**, 4068–4078.
66 K. Vandewal, K. Tvingstedt and O. Inganas, *Phys. Rev. B: Condens. Matter Mater. Phys.*, 2012, **86**, 035212-1–035212-9.
67 I. Riisness, C. Carach and M. J. Gordon, *Appl. Phys. Lett.*, 2012, **100**, 073308-1–073308-4.
68 M. Hallermann, I. Kriegel, E. Da Como, J. M. Berger, E. von Hauff and J. Feldmann, *Adv. Funct. Mater.*, 2009, **19**, 3662–3668.
69 C. Kästner, D. K. Susarova, R. Jadhav, C. Ulbricht, D. A. M. Egbe, S. Rathgeber, P. A. Troshin and H. Hoppe, *J. Mater. Chem.*, 2012, **22**, 15987–15997.
70 R. Jadhav, S. Tuerk, F. Kuehnlenz, V. Cimrova, S. Rathgeber, D. A. M. Egbe and H. Hoppe, *Phys. Status Solidi A*, 2009, **206**, 2695–2699.
71 C. R. Singh, M. Sommer, M. Himmerlich, A. Wicklein, S. Krischok, M. Thelakkat and H. Hoppe, *Phys. Status Solidi RRL*, 2011, **5**, 247–249.